Estimation of the mitochondrial membrane potential using fluorescence lifetime imaging microscopy

Irina A. Okkelman[1], Dmitri B. Papkovsky[1*], Ruslan I. Dmitriev[1,2*]

[1]Laboratory of Biophysics and Bioanalysis, ABCRF, School of Biochemistry and Cell Biology, University College Cork, Cork, Ireland

[2]Institute for Regenerative Medicine, I.M. Sechenov First Moscow State University, Moscow, Russian Federation

Running title: FLIM of the mitochondrial membrane potential

*to whom the correspondence should be addressed

Phone: 0214901698

e-mail: r.dmitriev@ucc.ie; d.papkovsky@ucc.ie

Funding

This work was supported by the Russian Science Foundation (RSF) grant 18-15-00407 (part 3.1, RID), Agilent University Research Program ACT-UR, No. 4225 (RID, DBP), Science Foundation Ireland (SFI) 13/SIRG/2144 (RID), 12/RC/2276 (DBP, IAO) and the Industry Fellowship 18/IF/6238 (RID) grants.

Abstract

Monitoring of cell metabolism represents important application area for the fluorescence lifetime imaging microscopy (FLIM). In particular, assessment of mitochondrial membrane potential (MMP) in complex three-dimensional multi-cellular *in vitro*, *ex vivo* and *in vivo* models would enable improved segmentation and functional discrimination of cell types, directly report on the mitochondrial function and complement the quenched-phosphorescence detection of cellular O_2 and two-photon excited FLIM of endogenous NAD(P)H. Here, we report the green and orange-emitting fluorescent dyes SYTO and tetramethylrhodamine methyl ester (TMRM) as potential FLIM probes for MMP. In addition to nuclear, SYTO 16 and 24 dyes also display mitochondrial accumulation. FLIM with the culture of human colon cancer HCT116 cells allowed observation of the heterogeneity of mitochondrial polarization during the cell cycle progression. The dyes also demonstrated good performance with 3D cultures of Lgr5-GFP mouse intestinal organoids, providing efficient and quick cell staining and compatibility with two-photon excitation. Multiplexed imaging of Lgr5-GFP, proliferating cells (Hoechst 33342-aided FLIM) and TMRM-FLIM allowed us to identify the population of metabolically active cells in stem cell niche. TMRM-FLIM enabled to visualize the differences in membrane potential between Lgr5-positive and other proliferating and differentiated cells. Altogether, SYTO 24 and TMRM dyes represent promising markers for advanced FLIM-based studies of cell bioenergetics with complex 3D and *in vivo* models.

Keywords: FLIM; Intestinal organoids; Lgr5-GFP; Mitochondrial membrane potential; SYTO; tetramethylrhodamine methyl ester;

Abbreviations

3D – three-dimensional; CBC – crypt base column cells; ECAR – extracellular acidification rate; FCCP – carbonyl cyanide p-trifluoromethoxyphenylhydrazone; FLIM – fluorescence lifetime imaging microscopy; GFP – green fluorescent protein; Lgr5 – leucine-rich repeat-containing G-protein coupled receptor 5; MMP – mitochondrial membrane potential; OCR – oxygen consumption rate; OxPhos – oxidative phosphorylation; PLIM – phosphorescence lifetime imaging microscopy; TMRM – tetramethylrhodamine methyl ester;

1. Introduction

Energy production and regulation of cell metabolism are essential for the living cell. Corresponding biomarkers are important for cancer, stem and basic cell biology, drug screening and discovery, cell death and toxicity, and tissue engineering (1-4). Quantitative assessment of cell metabolism and mitochondrial function is possible via a number of techniques, which include analyses of oxygenation and oxygen consumption rate, mitochondrial membrane potential (MMP), glycolytic flux, ATP and redox status, analysis of metabolome and other approaches (5-8). Photoluminescence (i.e. fluorescence and phosphorescence)-based methods enable quantification of these parameters in formats of a plate reader, fluorescence microscope and other readouts compatible with various cell and tissues. For *in vivo* and advanced microscopy applications, quantitative analysis of mitochondrial function is possible only by limited number of probes and approaches, such as measurement of cell oxygenation by phosphorescence quenching method (9,10), analysis of redox status by imaging of NAD(P)H, FAD^+ and tryptophan autofluorescence by FLIM and by using various genetically-encoded fluorescent biosensors (11-15). The quantitative assessment of the direct indicator of

mitochondrial function, MMP, remains a challenging task (16). This situation creates a gap in the recognized role of the mitochondrial dynamics (fusion and fission, local interactions with endoplasmic reticulum and other organelles) in the regulation of cell cycle, stem cell function and ageing (17-19) and the ability to study it. In particular, strong increase of MMP and hyperpolarization of mitochondria during G1/S transition are essential for normal progression of cell cycle (20).

Fluorescence lifetime imaging (FLIM) extends the capabilities of conventional microscopy by measuring the average time ('decay time'), which fluorophore spends in its excited state before emitting a photon (21,22). Thus, super-resolution microscopy (STED-FLIM) increases the number of simultaneously measured probes (23,24), while live cell FLIM allows quantitative measurement of O_2, pH, Ca^{2+}, NADH, cell cycle and other parameters (4,25-32). Current FLIM hardware enables fast measurements and is compatible with major microscopy platforms, one- and multiphoton excitation modes (4) and with emerging modalities such as light-sheet microscopy (33). In contrast to the 'traditional' intensity-based measurements, *in vivo* FLIM and PLIM allow visualization of oxygenation and metabolism in live animals (34-36), while *ex vivo* models benefit from the antibody-free labeling of proliferating cells, autofluorescence FLIM and related methods (26,27,37).

A number of dye structures including tetramethylrhodamine methyl ester (TMRM), Rhod123, JC-1, MitoTracker and cyanine dyes provide MMP-dependent staining of mammalian cells (16,38-42). Some of these dyes are fixable and preserve their localization after staining, while others are only usable with live cells. Many 'new' MMP dyes appear in the literature (43-45), but they often poorly characterized, show different staining patterns for different cell types and the rate of intracellular accumulation. Most of such dye structures, proteins and nanosensors targeting

mitochondria also require longer cell staining than conventional TMRM and Rhod123 probes. Very scarce data on evaluating these probes in FLIM and real-time MMP analyses are available; they include only two studies focused on FLIM with Rhod123, JC-1 and TMRM dyes (46,47).

Here, we report evaluation of the SYTO family and TMRM dyes as FLIM-based MMP probes. We found that with some optimization, SYTO 24 and TMRM dyes can inform on changes in mitochondrial polarization in 3D stem cell-derived intestinal organoid model in one- and multiphoton FLIM.

2. Materials and Methods

SYTO sampler kit S7572 (contains SYTO 11-14, 16, 21, 24, 25), Opti-MEM I medium, BCA protein assay, CellTiter-Glo kit, B27 and Lipofectamine 2000 were from ThermoFisher (Biosciences, Dublin, Ireland). O_2-sensitive nanoparticles NanO2 (PtTFPP-RL100) (48) and MM2 (49) were prepared as described previously. TagRFP-mito plasmid DNA was from Evrogen (Moscow, Russia). pH-Extra phosphorescent probe for ECAR assay was from Agilent Technologies (Little Island, Cork, Ireland). Hoechst 33342, tetramethylrhodamine methyl ester (TMRM), dimethyl sulfoxide (DMSO), FCCP, oligomycin, 5-Bromo-2'-deoxyuridine (BrdU), aphidicolin and all the other chemicals were from Sigma-Millipore (Dublin, Ireland). Re-usable multiwell silicon inserts were from Ibidi GmbH (Martinsried, Germany) and all the TC-grade sterile plastic was from Sarstedt (Dublin, Ireland).

Cell and organoid cultures

Human colon carcinoma HCT116 cells (ATCC) were cultured in McCoy 5A medium supplemented with 10% fetal bovine serum essentially as described previously (26).

Briefly, cells were passaged every 2-3 days and used for experiments between passages 8 and 20. For microscopy, cells were seeded onto collagen IV-pre-coated TC 35 mm dishes (Sarstedt) or collagen IV-poly-D-lysine – pre-coated multiwell coverglass-bottom inserts (Ibidi), allowed to reach 50-70% confluence and stained. For plate reader-based measurements, cells were seeded onto collagen IV-pre-coated 96-well plates (50-60,000 cells/ well on a day before the experiment) to reach 80-100% confluence and stained.

Staining was performed by diluting dyes or O_2-sensitive probes in the complete growth medium, incubation for required time (15 min-18 h) and washing with phenol red-free DMEM, supplemented with 10 mM glucose, 1 mM pyruvate, 2 mM l-Gln and 10 mM HEPES, pH 7.2 ('imaging medium'). Note that in most cases TMRM had to be present in the imaging medium.

Lgr5-GFP organoids (*Lgr5-EGFP-ires-CreERT2*) (50,51) were kindly provided by the laboratory of Prof. H. Clevers (Hubrecht Institute, The Netherlands) and were handled as described previously (52). For imaging, organoids were plated in reduced growth factor Matrigel onto 35 mm TC dishes and grown for 1-2 days prior to the analysis. Overnight incubation with 5 μM BrdU (18 h) and staining with TMRM, SYTO 24 and Hoechst 33342 dyes were performed in ENRVC medium representing Dulbecco's modified Eagle's medium nutrient mixture F-12 [HAM] supplemented with 1% penicillin/streptomycin, 1% N2, 2% B27, 1% GlutaMax, 1.25 mM NAC, EGF (50 ng/ml), R-spondin-1 (1 μg/ml), Noggin (100 ng/ml), 3 μM CHIR99021 and 1 mM sodium valproate. After staining, organoids were washed (if appropriate) and left in the Imaging medium.

Fixation with 4% paraformaldehyde was done essentially as described previously (52).

Widefield fluorescence microscopy

Preliminary evaluation of cell staining and co-localization with mitochondria were performed using inverted Zeiss Axiovert 200 microscope equipped with EC Plan Neofluar 40x/1.3 Oil and Plan Apochromat 100x/1.4 immersion objectives, pulsed excitation LED module (390 nm, 470 nm, 590 nm), gated CCD camera (LaVision BioTec) and integrated CO_2/O_2/T climate control chamber (PeCon) (53). SYTO dyes emission was collected by FITC filter cube (exc. 470 nm, em. 510-560 nm), TMRM emission was collected by TXRed-4040B-ZHE filter cube (Semrock, exc. 590 nm, em. 604-644 nm). Collected images were exported using ImSpector software (LaVision BioTec) as RGB TIFFs.

Laser-scanning (one-photon) TCSPC – FLIM and PLIM microscopies

FLIM and PLIM experiments with adherent HCT116 cells and intestinal organoids (multi-parameter FLIM of TMRM and Hoechst 33342) were performed on upright Zeiss Axio Examiner Z1 microscope equipped with water dipping 20x/1.0 and 63x/1.0 W-Plan Apochromat objectives, DCS-120 confocal scanner (Becker & Hickl GmbH), heated incubator / stage and motorized Z-axis control and 405 nm and 488 nm BDL-SMNI pulsed diode lasers (Becker & Hickl GmbH). Emission was collected using following settings: 635-675 nm filter (exc. 405 nm, PLIM, for NanO2), 438-458 nm filter (exc. 405 nm, FLIM, for Hoechst 33342), 512-536 nm filter (exc. 488 nm, FLIM, for GFP and SYTO dyes), 565-605 nm filter (exc. 488 nm, FLIM, for TMRM). FLIM (512x512 res.) and PLIM (256x256 res.) were performed essentially as described previously (26,27).

SYTO 24-stained intestinal organoids were analyzed on a white light laser (WLL)-equipped inverted Falcon FLIM TCS SP8 DMI8-CS system (Leica microsystems), with HC PL APO 63x/1.3 Glyc corr CS2 objective, HyD 2 detector and LAS X FLIM/FCS 3.5.5 software (Leica microsystems). SYTO 24 was imaged using 488 nm exc. (laser power 1.5-1.6 % for live, and 11% for fixed samples, emission collected at 505-578 nm, using 0-16 ns time gate, 1024x1024 res. and pinhole 103 μm).

Two-photon FLIM microscopy of intestinal organoids was performed on a 'Dive' Falcon FLIM TCS SP8 DM6B-Z-CFS multiphoton system, equipped with HC PL IRAPO 25x/1.00 water dipping objective, multiphoton lasers, HyD and HyD-RLD detectors, and LAS X 3.5.5 software (Leica microsystems). Emission of SYTO 24 was collected at 506-551 nm (exc. 919 nm, 6.1% laser power), emission of Hoechst 33342 was collected at 394-455 nm (exc. 700 nm, 5.9% laser power, 512x512, pinhole 55.7 μm).

Assessment of effects of SYTO 24 and TMRM on cell bioenergetics

Effects of long (17 h) and short-term (20 min) incubation effects of SYTO 24 (0.1 μM) and TMRM (10 nM) on the bioenergetics were analyzed using previously described plate reader-based platform (7,54) measuring oxygen consumption rate (OCR), glycolytic flux-mediated extracellular acidification (ECAR) and total cellular ATP (CellTiter-Glo assay kit, Promega). Typically, cells were grown on 96-well plates, incubated with SYTO 24 and TMRM dyes and immediately proceeded to measurements with MM2 probe (0.5 μg/ml, OCR under oil) or pH-Extra probe (with 1.5 h pre-incubation in CO_2-free conditions, ECAR) in the presence of drugs (DMSO

(mock) or 1 μM FCCP, 10 μM oligomycin) over 1.5 h (37 ^{o}C). ECAR samples were subjected to ATP assay and protein extraction and analysis (BCA protein assay kit).

Data assessment and statistics

FLIM data were initially processed in SPCImage (Becker & Hickl) or LAS X (Leica) software to optimize fitting decay algorithms ($\chi 2 < 1.5$) and perform calculation of FLIM images for whole imaged area or selected Regions of Interest (ROI). Typical fitting (data trace, IRF, fit), ASCII matrices of photon counts (intensity) or fluorescence lifetimes (color coded values), RGB TIFF images and distribution histograms were exported and analyzed in Microsoft Excel or Origin 6.0. 3D reconstructions of FLIM data were performed in LAS X 3.5.5 software (Leica Microsystems). Plate reader data representing the replicates from the separate wells, were tested for statistical significance using independent *t*-test (normal distribution).

3. Results

3.1. SYTO dyes demonstrate non-exclusively nuclear staining in live mammalian cells

In search of a green nuclear live FLIM probe we turned our attention to the SYTO family of dyes (Molecular Probes^{TM}). Based on reviews (55,56) and previous report on FRET between SYTO 13 and Hoechst 33342 dyes (57) we expected to see SYTO dyes as green fluorescent probes with exclusively nuclear localization. However, when we stained human colon carcinoma HCT116 cells with SYTO 16 we also observed cytoplasmic localization (Fig. 1A). Closer look at the extranuclear localization pointed at mitochondrial co-localization, in agreement with the previous study (58). Fluorescence lifetime analysis of SYTO 16 and 24 revealed differences

between cytoplasmic and nuclear pools, with longer fluorescence lifetimes (4-4.5 ns) found in nuclei (Fig. 1B). Co-staining with TMRM confirmed partial co-localization between cytoplasmic pools of SYTO 16 and 24 and mitochondria in resting HCT116 cells (Fig. 1C).

We then looked if the mitochondrial accumulation of SYTO dyes depended on the MMP. Treatment with uncoupler FCCP revealed a response, reflecting re-distribution of the SYTO 16 and 24 from mitochondria into nucleus. This re-localization affected fluorescence lifetime distribution histograms and increased the nuclear fraction (Fig. 1B). To elaborate this observation, we tested other SYTO dyes (Figs. 1, S1) for their response to the mitochondrial uncoupling and compared them with TMRM. Surprisingly, none of them demonstrated clear nuclear localization in live resting cells, while SYTO 16, 21, 24 and 25 displayed nuclear re-localization in cells with depolarized mitochondria. This re-localization was slower than for TMRM (2-5 min) and depended on cell loading time and staining concentration.

The complex pattern of interaction of SYTO dyes with cellular biomolecules (e.g. proteins, RNA and DNA) can be influenced by their charge and/ or pH. Thus, in unhealthy, stressed and fixed cells (not shown), nuclear localization of SYTO dyes was observed, in agreement with the previous microscopy and FACS data (55,59).

3.2. Dose-dependence of staining and its effect on cell bioenergetics

We next studied the time- and concentration dependence of fluorescence lifetime of SYTO 16, 24 and TMRM dyes in cultured cells. We found that when used at low ‘unquenched’ concentrations of 10-30 nM, fluorescence lifetime of TMRM in mitochondria was drifting and decreasing over time (Fig.2A, B), due to ongoing mitochondrial accumulation from the medium and increased self-quenching. Thus, its

withdrawal from assay media could be beneficial for the short-term (15-25 min) experiments. We found that 10 nM staining concentration gave satisfactory stability of the mean lifetimes if the probe was withdrawn from solution. On the other hand, 30 nM could give better resolution in fluorescence lifetime when present in the assay medium (Fig. 2B).

SYTO 16 and 24 (do not have to be present in assay medium during imaging) showed high brightness allowing their use at submicromolar concentrations, and long decay times (2.5~4 ns and 3.5~4.5 ns respectively) providing suitability for multiplexing with other green dyes, such as EGFP (~2.4 ns). However, the complex pattern on intracellular distribution of SYTO 24 made the analysis of dose-dependence of lifetime difficult (Fig. 3). Both nuclear and mitochondrial pools of SYTO 24 depended on staining concentration, with overall tendency for stronger nuclear staining with higher concentrations. Such complex distribution was reflected in distribution histograms for the whole stained cells (Fig. 3B-C). Similar data were obtained with SYTO 16 (not shown). Potentially, high concentrations of SYTO dyes also influenced the mitochondria upon prolonged staining: cells frequently showed reduced mitochondrial localization and response to FCCP.

Since the MMP can drastically change during cell cycle and mitochondria fusion processes, we looked if we could observe the previously reported hyperpolarization of the mitochondria at the G1/S border (20). Thus, a range of fluorescence lifetimes observed in mitochondria of asynchronous culture could be explained by different stages of the cell cycle. Indeed, cells synchronized in G1 and S phases demonstrated decreased fluorescence lifetimes reflecting increased membrane polarization (Fig. S2).

We wondered if staining with SYTO and TMRM dyes has any effect on cell bioenergetics. Thus, we looked at the changes in oxygen consumption rate, glycolysis-mediated extracellular acidification and total cellular ATP (Fig. 4). We found that SYTO 24 and TMRM influenced OxPhos even upon 20 min staining, but this effect did not increase after 17 h incubation. These dyes seemingly caused mild uncoupling, acidification and activation of respiration reflected in slight increase of ATP. The partial 'self-induced' nuclear translocation of SYTO dyes (Fig. 3) supports the assumption on mild uncoupling by SYTO and TMRM dyes. This data are in agreement with the previously reported effect of TMRM on mitochondrial respiration (42). Since these effects on cell bioenergetics were not inhibitory we concluded that SYTO 24 and TMRM could be applied in further physiological studies.

3.3. FLIM analysis of mitochondrial potential in cultured cells and 3D model of Lgr5-GFP stem cell-derived intestinal organoids

To test the feasibility of FLIM for monitoring of mitochondrial membrane potential, we first looked at changes in TMRM fluorescence intensity and lifetime upon uncoupling with adherent HCT116 cells. The sequential addition of DMSO (mock) and 2 μM FCCP to the cells demonstrated expected (42) re-distribution of the dye and its dissipation from the mitochondria (Fig. S3). FLIM analysis also demonstrated progressive changes in fluorescence lifetime, indicative to the FCCP action (red histograms on Fig. S3C). The changes in decay time differed depending on the time post dissipation, e.g. aggregated dye regions showed overall increase of lifetime (Fig. 1B). We also compared TMRM-FLIM with the monitoring of cell oxygenation at similar cell densities using O_2-PLIM method with NanO2 probe (48,53). (Fig. S3E, F). NanO2-stained cells displayed lysosomal-like localization in agreement with

previous observations (60) and some aggregation visible as ‘hypoxic’ (long emission lifetimes) regions. While some selected ROIs did show transient decrease in intracellular oxygenation due to FCCP action, the whole imaged area distribution histograms showed minor or no response to the uncoupler.

The complex 3D environment can enable advanced use of ‘dissipation dyes’ TMRM and SYTO, since during uncoupling the loss of dye from depolarized mitochondria would occur not just into medium but also into neighboring cells. The intestinal organoid model recapitulating most of the functions of the native epithelium harbors many different cell types with differences in bioenergetics and proliferation (61). We chose the culture of mouse intestinal organoids harboring Lgr5-GFP (50,51), where stem cells are constantly labeled by the GFP and gradually lose it during the process of differentiation.

TMRM staining revealed striking differences in cytoplasmic fractions of fluorescence lifetimes in organoids (Fig. 5). Taking advantage of Hoechst 33342-BrdU FLIM method of labeling of cell proliferation (26) and labeling of Lgr5+ cells with GFP, we identified the population of cells with high MMP (shorter fluorescence lifetimes), residing in the stem cell niche (Fig. 5A). The long labeling with BrdU (18 h) and subsequent FLIM of Hoechst 33342 confirmed that Lgr5-GFP+ cells and the cells, which recently lost GFP expression, belonged to the amplification zones in organoids. Interestingly, most of differentiated enterocyte-like cells localized close to the lumen regions (no GFP, no proliferation) had very diffuse TMRM staining indicating lower mitochondrial polarization.

We next explored the effect of FCCP uncoupling on the different cell types in the organoids. Regions 1 and 2 compared to 3 and 4 (Fig. 5B-F) did not significantly change their fluorescence intensities during treatments (Fig. 5D), but the changes in

fluorescence lifetimes were seen (Fig. 5F). These four selected regions co-localized with Lgr5-GFP and resided in the amplification zone (not shown). Thus, TMRM-FLIM method allowed discrimination of the two metabolically different cell types within the stem cell niche, potentially differing in their stage of cell cycle (for 1 and 2) or other features.

We also tested the applicability of SYTO 24 for FLIM of intestinal organoids (Fig. 6). Despite its minor toxicity in 2D cancer cell cultures, we did not see any acute effects on Lgr5-GFP organoids. The fixation led to complete translocation of SYTO 24 into nuclei, making it useful only as nuclear stain (Fig. 6A). Live organoids displayed bright staining (overlapping with weaker fluorescence of Lgr5-GFP cells) of the nuclei and cytoplasm, similar to our FLIM data (Fig. 6B, 1). Stained cells in organoids had mitochondrial and nuclear fractions with distinct emission lifetimes (Fig. 6C,D). Some poorly stained cells with features of Paneth cells were also observed. Fig. 6E,F demonstrates that FLIM with SYTO 24 dye is also applicable for advanced analysis of organoid function in 3D. Using two-photon excited FLIM we also combined detection of cell proliferation (Hoechst 33342-BrdU labeling-based FLIM (26)) and staining with SYTO 24 (Fig. S4). The micro-regions within intestinal organoids were co-labeled with Hoechst 33342 without adverse effects of SYTO 24 staining.

4. Discussion

In present paper, we described new applications of live cell imaging dyes SYTO 16, 24 and TMRM as FLIM probes to study mitochondrial membrane potential (MMP). The mitochondrial accumulation of the SYTO dyes helped to use them for FLIM-based analysis of MMP. Until now, SYTO dyes were mainly used in flow cytometry,

i.e. when the cells can frequently become stressed and become round in shape. We observed that the dyes SYTO 13, 16, 21, 24 localize to nuclei only after dissipation of the MMP by mitochondrial uncoupling or by other treatments. Mitochondrial localization of SYTO 16 and 24 was only partial and confined to some focal points (Fig. 1). Further studies by super-resolution microcopy or related approaches can help better understanding of their mitochondrial attachment and trafficking. The lack of structural knowledge for these dyes prevents the understanding of physical-chemical basis of their interaction with mitochondria.

Interestingly, chosen SYTO and TMRM dyes shared some common features as FLIM probes: they showed dose-dependence of fluorescence lifetime (e.g. shorter lifetime due to quenching at higher mitochondrial polarization) and release from the mitochondria upon depolarization (Fig. 2, 3). SYTO 24 and TMRM also affected mitochondrial respiration, most likely due to their mild uncoupling effects on cell function (Fig. 4). This effect was previously reported for TMRM and some other MMP probes (42), but is rarely taken into account. Further optimization and use of improved more sensitive imaging platforms can enable wider use of these dyes in MMP analysis by FLIM.

Described dyes also display useful range of fluorescence lifetimes, especially SYTO 24 and 16, providing good dynamic range and sensitivity to MMP changes (Fig. 2,3), useful for multiplexing with many other dyes in time-domain, under one- or two-photon excitation modes. The relatively fast loading of intestinal organoids (Fig. 5-6) makes these dyes well suited for staining of 3D tissue models, *ex vivo* specimens or topical application *in vivo*. SYTO and TMRM differ spectrally, so they can be also used as a dual referenced FRET-FLIM system for MMP or live cell tracing. On the other hand, their complex pattern of interaction with intracellular compartments and

re-distribution upon MMP dissipation do not allow ‘absolute’ FLIM calibrations, making them semi-quantitative. Still, measurement of fluorescence lifetimes brings another dimension and complements the intensity-based MMP measurements. Tested dyes not only produce changes in overall brightness but also detected heterogeneity of mitochondrial polarization at resting conditions (Figures 2, 3, 5, S2).

Our study also demonstrates the use of 3D tissue model of stem cell-derived intestinal organoids with these dyes in FLIM mode. Redistribution of the probe accumulation, a frequent obstacle with 2D cell cultures, can become a useful feature in 3D. Thus, continuous changes in the MMP within the organoid did not lead to the loss of the dye to the medium but enabled functional discrimination between the different cell types (Fig. 5). Co-localization analysis of TMRM-stained cells in FLIM with Lgr5-GFP-labeled proliferating cells allowed tracing of the different cells within intestinal crypts accordingly to their mitochondrial function. These results are in line with findings by Rodriguez-Colman and co-workers, who used JC-1 staining to detect mitochondrial polarization (61), although our results from TMRM-FLIM point that ENRVC-grown cells residing in the crypts can be more heterogeneous and also represent quiescent or non-proliferating cells in G1/S phase (Fig. 5).

Staining of intestinal organoids with SYTO 24 also visualized the mitochondria, similar to the cultured cells (Fig. 6). However, analysis of SYTO 24-stained organoids requires imaging systems with high resolution and contrast, optical sectioning, such as two-photon excitation with improved Z resolution or use of smaller sized samples.

We found SYTO 24 and TMRM well suitable for multi-parametric FLIM analysis of intestinal organoids (Fig. 5-6, S4). These dyes can be combined with analysis of oxygenation by PLIM probes (27), biosensor scaffold materials (25,62) or other fluorescent biosensors. However, we found that TMRM staining can be difficult to

combine with two-photon excited FLIM imaging of NADH, due to the very high brightness of TMRM and its broad excitation range (data not shown). Altogether, presented dyes are applicable to the FLIM analysis of 3D tissue models, spheroids, cell aggregates and organoids, while *in vivo* applications may require additional optimization of staining and delivery route.

Acknowledgments

We thank Dr. Heiko Dussmann (RCSI, Dublin) for providing initial stock of SYTO 16 dye, Dr. Heike Glauner (Leica microsystems) for support with Leica SP8 Falcon FLIM measurements and data analysis, and Jens Puschhof (Hubrecht Institute) for help and support with Lgr5-GFP organoid culture.

References

1. Zhang H, Ryu D, Wu Y, Gariani K, Wang X, Luan P, D'Amico D, Ropelle ER, Lutolf MP, Aebersold R. NAD+ repletion improves mitochondrial and stem cell function and enhances life span in mice. Science 2016;352:1436-1443.
2. Rossignol R, Gilkerson R, Aggeler R, Yamagata K, Remington SJ, Capaldi RA. Energy substrate modulates mitochondrial structure and oxidative capacity in cancer cells. Cancer research 2004;64:985-993.
3. Teslaa T, Teitell MA. Pluripotent stem cell energy metabolism: an update. The EMBO journal 2015;34:138-153.
4. Dmitriev RI. Multi-Parametric Live Cell Microscopy of 3D Tissue Models: Springer; 2017.
5. Brand MD, Nicholls DG. Assessing mitochondrial dysfunction in cells. Biochemical Journal 2011;435:297-312.
6. Foster KA, Galeffi F, Gerich FJ, Turner DA, Müller M. Optical and pharmacological tools to investigate the role of mitochondria during oxidative stress and neurodegeneration. Progress in neurobiology 2006;79:136-171.
7. Zhdanov A, Favre C, O'Flaherty L, Adam J, O'Connor R, Pollard P, Papkovsky D. Comparative bioenergetic assessment of transformed cells using a cell energy budget platform. Integrative Biology 2011;3:1135-1142.
8. Wu M, Neilson A, Swift AL, Moran R, Tamagnine J, Parslow D, Armistead S, Lemire K, Orrell J, Teich J. Multiparameter metabolic analysis reveals a close link between attenuated mitochondrial bioenergetic function and enhanced glycolysis dependency in human tumor cells. American Journal of Physiology-Cell Physiology 2007;292:C125-C136.

9. Dmitriev RI, Papkovsky DB. Quenched-phosphorescence detection of molecular oxygen: applications in life sciences: Royal Society of Chemistry; 2018.
10. Papkovsky DB, Dmitriev RI. Biological detection by optical oxygen sensing. Chemical Society Reviews 2013;42:8700-8732.
11. Wallrabe H, Svindrych Z, Alam SR, Siller KH, Wang T, Kashatus D, Hu S, Periasamy A. Segmented cell analyses to measure redox states of autofluorescent NAD (P) H, FAD & Trp in cancer cells by FLIM. Scientific reports 2018;8:79.
12. Blacker TS, Mann ZF, Gale JE, Ziegler M, Bain AJ, Szabadkai G, Duchen MR. Separating NADH and NADPH fluorescence in live cells and tissues using FLIM. Nature communications 2014;5:3936.
13. Ma N, Digman MA, Malacrida L, Gratton E. Measurements of absolute concentrations of NADH in cells using the phasor FLIM method. Biomedical optics express 2016;7:2441-2452.
14. Lakowicz JR, Szmacinski H, Nowaczyk K, Johnson ML. Fluorescence lifetime imaging of free and protein-bound NADH. Proceedings of the National Academy of Sciences 1992;89:1271-1275.
15. Mongeon R, Venkatachalam V, Yellen G. Cytosolic NADH-NAD+ redox visualized in brain slices by two-photon fluorescence lifetime biosensor imaging. Antioxidants & redox signaling 2016;25:553-563.
16. Nicholls DG. Fluorescence Measurement of Mitochondrial Membrane Potential Changes in Cultured Cells. Mitochondrial Bioenergetics: Springer; 2018. p 121-135.
17. Correia‐Melo C, Marques FD, Anderson R, Hewitt G, Hewitt R, Cole J, Carroll BM, Miwa S, Birch J, Merz A. Mitochondria are required for pro‐ageing features of the senescent phenotype. The EMBO journal 2016;35:724-742.
18. Schrepfer E, Scorrano L. Mitofusins, from mitochondria to metabolism. Molecular cell 2016;61:683-694.
19. Chen H, Chan DC. Mitochondrial dynamics in regulating the unique phenotypes of cancer and stem cells. Cell metabolism 2017;26:39-48.
20. Mitra K, Wunder C, Roysam B, Lin G, Lippincott-Schwartz J. A hyperfused mitochondrial state achieved at G₁–S regulates cyclin E buildup and entry into S phase. Proceedings of the National Academy of Sciences 2009;106:11960-11965.
21. Berezin MY, Achilefu S. Fluorescence lifetime measurements and biological imaging. Chemical reviews 2010;110:2641-2684.
22. Levitt JA, Matthews DR, Ameer-Beg SM, Suhling K. Fluorescence lifetime and polarization-resolved imaging in cell biology. Current opinion in biotechnology 2009;20:28-36.
23. Lenz M, Brown A, Auksorius E, Davis D, Dunsby C, Neil M, French P. A STED-FLIM microscope applied to imaging the natural killer cell immune synapse. 2011. International Society for Optics and Photonics. p 79032D.
24. Niehörster T, Löschberger A, Gregor I, Krämer B, Rahn H-J, Patting M, Koberling F, Enderlein J, Sauer M. Multi-target spectrally resolved fluorescence lifetime imaging microscopy. Nature methods 2016;13:257.
25. O'Donnell N, Okkelman IA, Timashev P, Gromovykh TI, Papkovsky DB, Dmitriev RI. Cellulose-based scaffolds for fluorescence lifetime imaging-assisted tissue engineering. Acta biomaterialia 2018;80:85-96.

26. Okkelman IA, Dmitriev RI, Foley T, Papkovsky DB. Use of fluorescence lifetime imaging microscopy (FLIM) as a timer of cell cycle S phase. PloS one 2016;11:e0167385.
27. Okkelman IA, Foley T, Papkovsky DB, Dmitriev RI. Live cell imaging of mouse intestinal organoids reveals heterogeneity in their oxygenation. Biomaterials 2017;146:86-96.
28. Poëa-Guyon S, Pasquier H, Mérola F, Morel N, Erard M. The enhanced cyan fluorescent protein: a sensitive pH sensor for fluorescence lifetime imaging. Analytical and bioanalytical chemistry 2013;405:3983-3987.
29. Sarder P, Maji D, Achilefu S. Molecular probes for fluorescence lifetime imaging. Bioconjugate chemistry 2015;26:963-974.
30. Jenkins J, Borisov SM, Papkovsky DB, Dmitriev RI. Sulforhodamine nanothermometer for multiparametric fluorescence lifetime imaging microscopy. Analytical chemistry 2016;88:10566-10572.
31. Niesner R, Peker B, Schlüsche P, Gericke KH. Noniterative biexponential fluorescence lifetime imaging in the investigation of cellular metabolism by means of NAD (P) H autofluorescence. ChemPhysChem 2004;5:1141-1149.
32. Papkovsky DB, Dmitriev RI. Imaging of oxygen and hypoxia in cell and tissue samples. Cellular and molecular life sciences 2018;75:2963-2980.
33. Greger K, Neetz MJ, Reynaud EG, Stelzer EH. Three-dimensional fluorescence lifetime imaging with a single plane illumination microscope provides an improved signal to noise ratio. Optics express 2011;19:20743-20750.
34. Conway JR, Warren SC, Herrmann D, Murphy KJ, Cazet AS, Vennin C, Shearer RF, Killen MJ, Magenau A, Mélénec P. Intravital imaging to monitor therapeutic response in moving hypoxic regions resistant to PI3K pathway targeting in pancreatic cancer. Cell reports 2018;23:3312-3326.
35. Conway JR, Warren SC, Timpson P. Context-dependent intravital imaging of therapeutic response using intramolecular FRET biosensors. Methods 2017;128:78-94.
36. Sakadžić S, Roussakis E, Yaseen MA, Mandeville ET, Srinivasan VJ, Arai K, Ruvinskaya S, Devor A, Lo EH, Vinogradov SA. Two-photon high-resolution measurement of partial pressure of oxygen in cerebral vasculature and tissue. Nature methods 2010;7:755.
37. Walsh AJ, Cook RS, Sanders ME, Aurisicchio L, Ciliberto G, Arteaga CL, Skala MC. Quantitative optical imaging of primary tumor organoid metabolism predicts drug response in breast cancer. Cancer research 2014;74:5184-5194.
38. Reers M, Smiley ST, Mottola-Hartshorn C, Chen A, Lin M, Chen LB. [29] Mitochondrial membrane potential monitored by JC-1 dye. Methods in enzymology. Volume 260: Elsevier; 1995. p 406-417.
39. Johnson LV, Walsh ML, Bockus BJ, Chen LB. Monitoring of relative mitochondrial membrane potential in living cells by fluorescence microscopy. The Journal of Cell Biology 1981;88:526-535.
40. Mathur A, Hong Y, Kemp BK, Barrientos AA, Erusalimsky JD. Evaluation of fluorescent dyes for the detection of mitochondrial membrane potential changes in cultured cardiomyocytes. Cardiovascular Research 2000;46:126-138.
41. Chen LB. Fluorescent labeling of mitochondria. Methods in cell biology. Volume 29: Elsevier; 1988. p 103-123.

42. Scaduto RC, Grotyohann LW. Measurement of Mitochondrial Membrane Potential Using Fluorescent Rhodamine Derivatives. Biophysical Journal 1999;76:469-477.
43. Press AT, Ungelenk L, Rinkenauer AC, Gröger M, Lehmann F, Mosig A, Schubert US, Clemens MG, Bauer M. A new fluorescent dye for cell tracing and mitochondrial imaging in vitro and in vivo. Journal of biophotonics 2016;9:888-900.
44. Šarić A, Crnolatac I, Bouillaud F, Sobočanec S, Mikecin A-M, Šafranko ŽM, Delgeorgiev T, Piantanida I, Balog T, Petit PX. Non-toxic fluorescent phosphonium probes to detect mitochondrial potential. Methods and applications in fluorescence 2017;5:015007.
45. Liu W, Zhou B, Niu G, Ge J, Wu J, Zhang H, Xu H, Wang P. Deep-red emissive crescent-shaped fluorescent dyes: substituent effect on live cell imaging. ACS applied materials & interfaces 2015;7:7421-7427.
46. Pohl EE, Schueler J, Rupprecht A. Mitochondrial Membrane Potential in Living Neurons Measured by Flim. Biophysical Journal 2011;100:248a.
47. Evans N, Gnudi L, Rolinski O, Birch D, Pickup J. Glucose-dependent changes in NAD (P) H-related fluorescence lifetime of adipocytes and fibroblasts in vitro: potential for non-invasive glucose sensing in diabetes mellitus. Journal of Photochemistry and Photobiology B: Biology 2005;80:122-129.
48. Fercher A, Borisov SM, Zhdanov AV, Klimant I, Papkovsky DB. Intracellular O2 sensing probe based on cell-penetrating phosphorescent nanoparticles. ACS nano 2011;5:5499-5508.
49. Kondrashina AV, Dmitriev RI, Borisov SM, Klimant I, O'Brien I, Nolan YM, Zhdanov AV, Papkovsky DB. A phosphorescent nanoparticle‐based probe for sensing and imaging of (intra) cellular oxygen in multiple detection modalities. Advanced Functional Materials 2012;22:4931-4939.
50. Barker N, Van Es JH, Kuipers J, Kujala P, Van Den Born M, Cozijnsen M, Haegebarth A, Korving J, Begthel H, Peters PJ. Identification of stem cells in small intestine and colon by marker gene Lgr5. Nature 2007;449:1003.
51. Sato T, Vries RG, Snippert HJ, Van De Wetering M, Barker N, Stange DE, Van Es JH, Abo A, Kujala P, Peters PJ. Single Lgr5 stem cells build crypt–villus structures in vitro without a mesenchymal niche. Nature 2009;459:262.
52. Okkelman IA, Foley T, Papkovsky DB, Dmitriev RI. Multi-Parametric Imaging of Hypoxia and Cell Cycle in Intestinal Organoid Culture. In: Dmitriev R, editor. Multi-Parametric Live Cell Microscopy of 3D Tissue Models. Volume 1035. Springer, Cham: Advances in Experimental Medicine and Biology; 2017. p 85-103.
53. Dmitriev RI, Zhdanov AV, Nolan YM, Papkovsky DB. Imaging of neurosphere oxygenation with phosphorescent probes. Biomaterials 2013;34:9307-9317.
54. Dmitriev RI, Borisov SM, Düssmann H, Sun S, Müller BJ, Prehn J, Baklaushev VP, Klimant I, Papkovsky DB. Versatile conjugated polymer nanoparticles for high-resolution O2 imaging in cells and 3D tissue models. ACS nano 2015;9:5275-5288.
55. Wlodkowic D, Skommer J, Faley S, Darzynkiewicz Z, Cooper JM. Dynamic analysis of apoptosis using cyanine SYTO probes: from classical to microfluidic cytometry. Experimental cell research 2009;315:1706-1714.

56. Atale N, Gupta S, Yadav U, Rani V. Cell‐death assessment by fluorescent and nonfluorescent cytosolic and nuclear staining techniques. Journal of microscopy 2014;255:7-19.
57. Pelicci S, Oneto M, Di Bona M, Diaspro A, Lanzanò L. FLIM-FRET of Chromatin in Live Cells using Two DNA-Binding Dyes. Biophysical Journal 2018;114:532a.
58. Bruce JI, Giovannucci DR, Blinder G, Shuttleworth TJ, Yule DI. Modulation of [Ca2+] i signaling dynamics and metabolism by perinuclear mitochondria in mouse parotid acinar cells. Journal of Biological Chemistry 2004;279:12909-12917.
59. Herman P, Maliwal B, Lin HJ, Lakowicz J. Frequency‐domain fluorescence microscopy with the LED as a light source. Journal of Microscopy 2001;203:176-181.
60. Dmitriev RI, Zhdanov AV, Jasionek G, Papkovsky DB. Assessment of cellular oxygen gradients with a panel of phosphorescent oxygen-sensitive probes. Analytical chemistry 2012;84:2930-2938.
61. Rodríguez-Colman MJ, Schewe M, Meerlo M, Stigter E, Gerrits J, Pras-Raves M, Sacchetti A, Hornsveld M, Oost KC, Snippert HJ. Interplay between metabolic identities in the intestinal crypt supports stem cell function. Nature 2017;543:424.
62. Jenkins J, Dmitriev RI, Morten K, McDermott KW, Papkovsky DB. Oxygen-sensing scaffolds for 3-dimensional cell and tissue culture. Acta Biomaterialia 2015;16:126-135.

Figures and figure legends

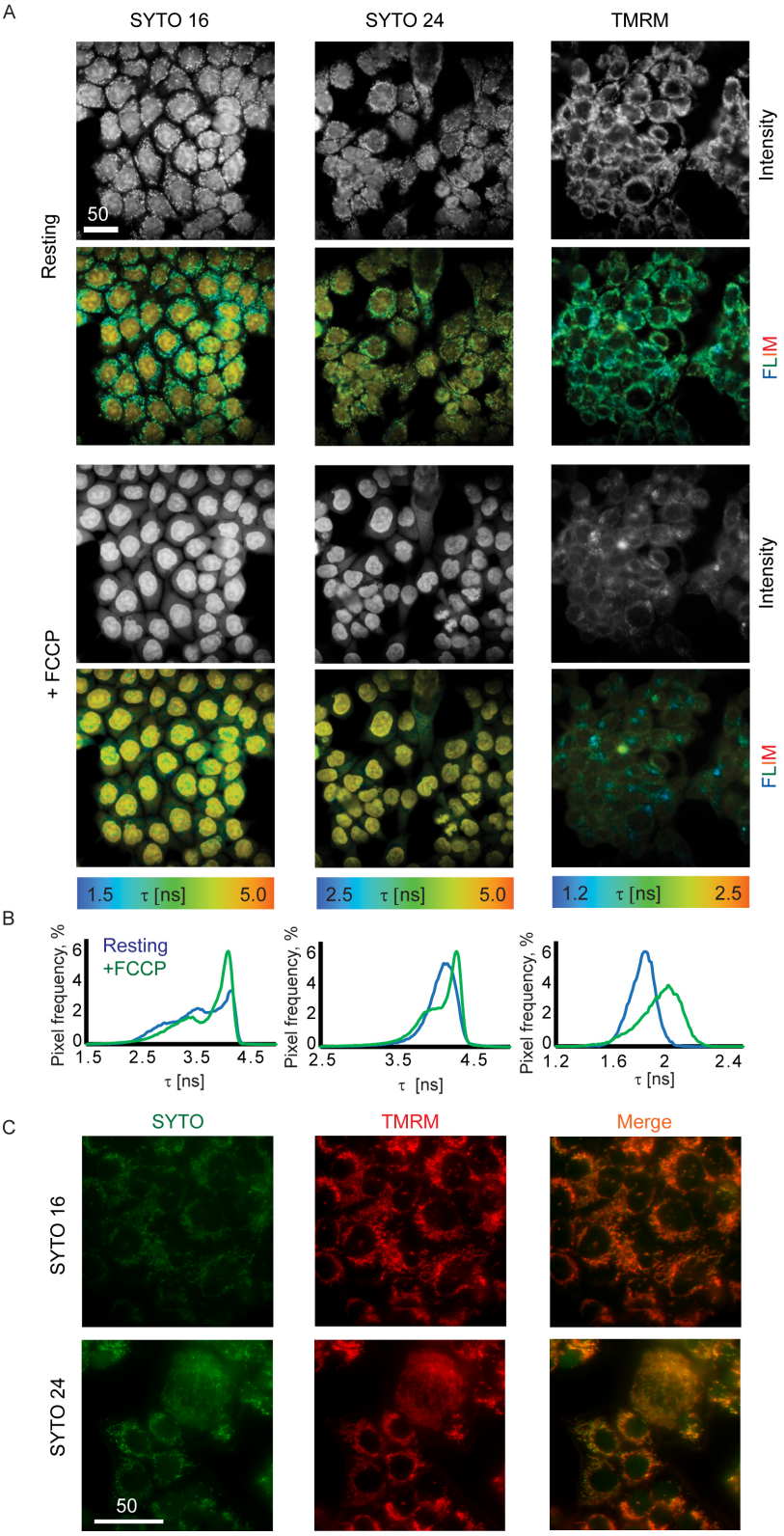

Figure 1. Fluorescence intensity and lifetime (FLIM) microscopy reveal complex staining pattern of live HCT116 cells with SYTO 16, 24 (0.1 μM, 1 h, then washing) and TMRM (10

nM, 15 min, no washing) dyes, imaged at rest and after FCCP (2 μM, 5 min) addition. A: (from top to bottom) fluorescence intensity (grayscale) and lifetime (color) images, at rest and after FCCP addition. B: fluorescence lifetime distribution histograms for A. C: partial co-localization between SYTO 16 and 24 and mitochondrial TMRM dyes. Scale bar is in μm.

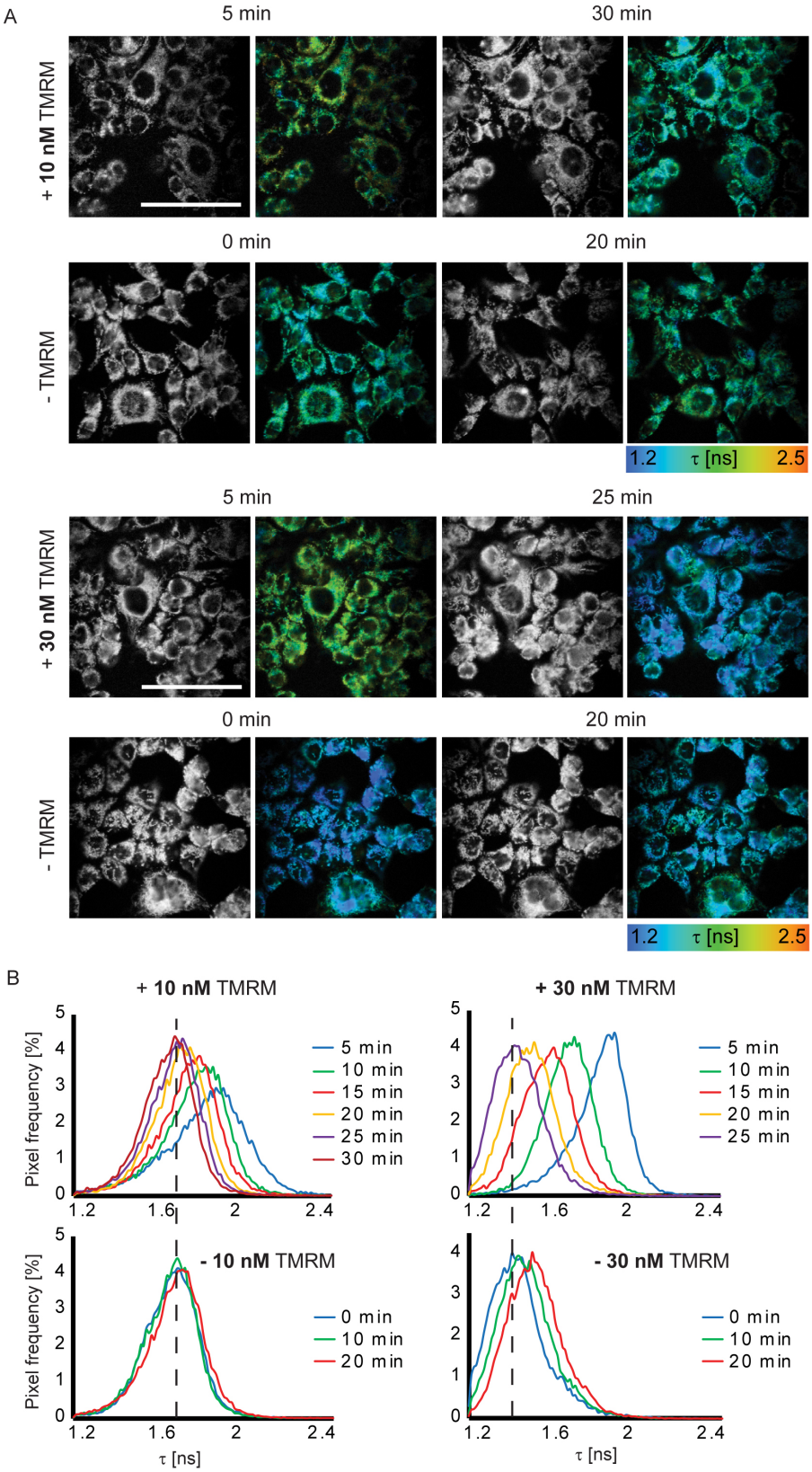

Figure 2. Dose- and time dependence of TMRM fluorescence lifetime in cultured HCT116 cells. HCT116 cells were stained with different concentrations of TMRM (present "+" or absent in the imaging media, "-") and imaged at different time points post-staining. A:

examples of FLIM images for 10 and 30 nM concentrations (+/- TMRM). B: respective distribution histograms. Scale bar is 50 µm.

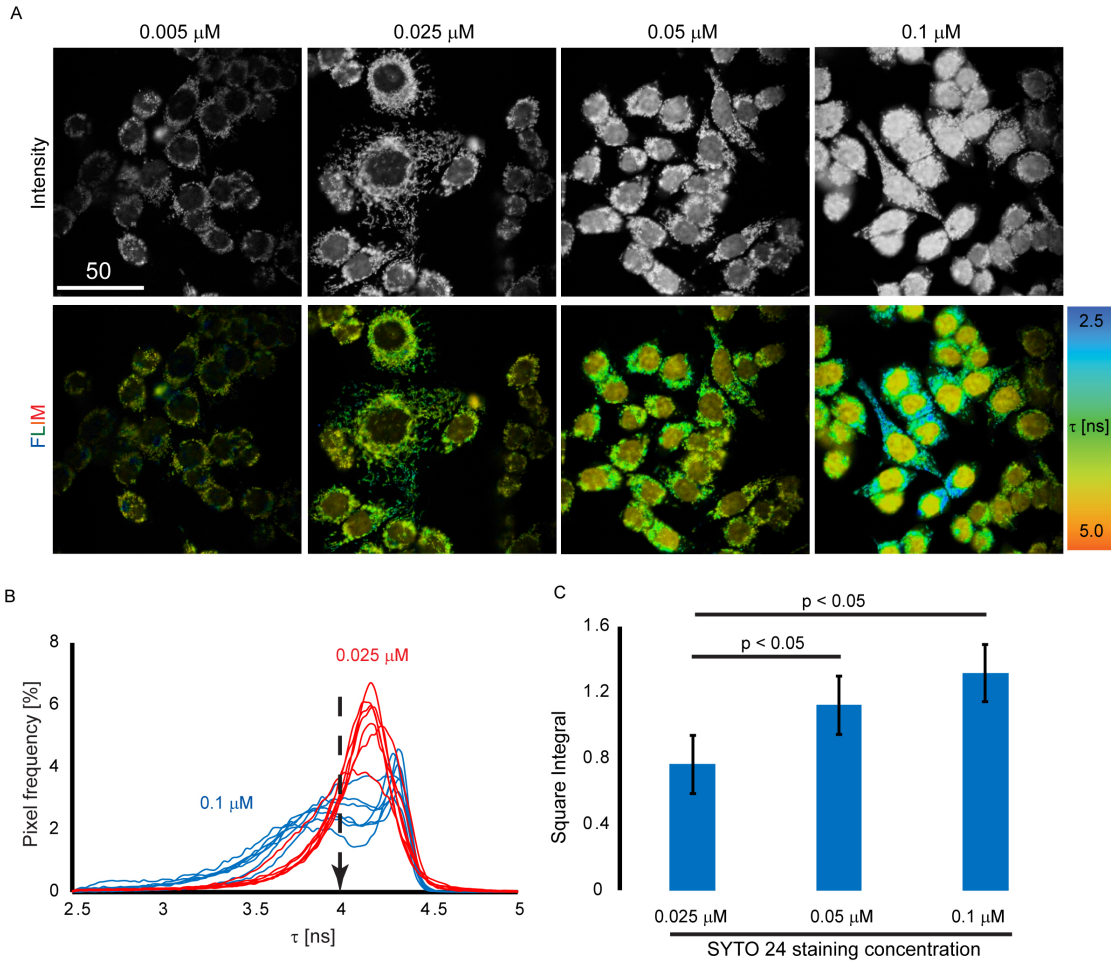

Figure 3. Dose-dependence of effect of SYTO 24 staining on fluorescence lifetime in HCT116 cells. Cells were stained with different concentrations of SYTO 24 (30 min) and washed before imaging. A: intensity (gray scale) and fluorescence lifetime (color) images of cells. B: example of variability of observed fluorescence lifetime distribution histograms and (C) integral of frequency of τ= 4 ns for different staining conditions (statistical differences were analyzed by independent *t*-test; groups of 0.05 µM and 0.1 µM did not show meaningful differences). Scale bar is 50 µm.

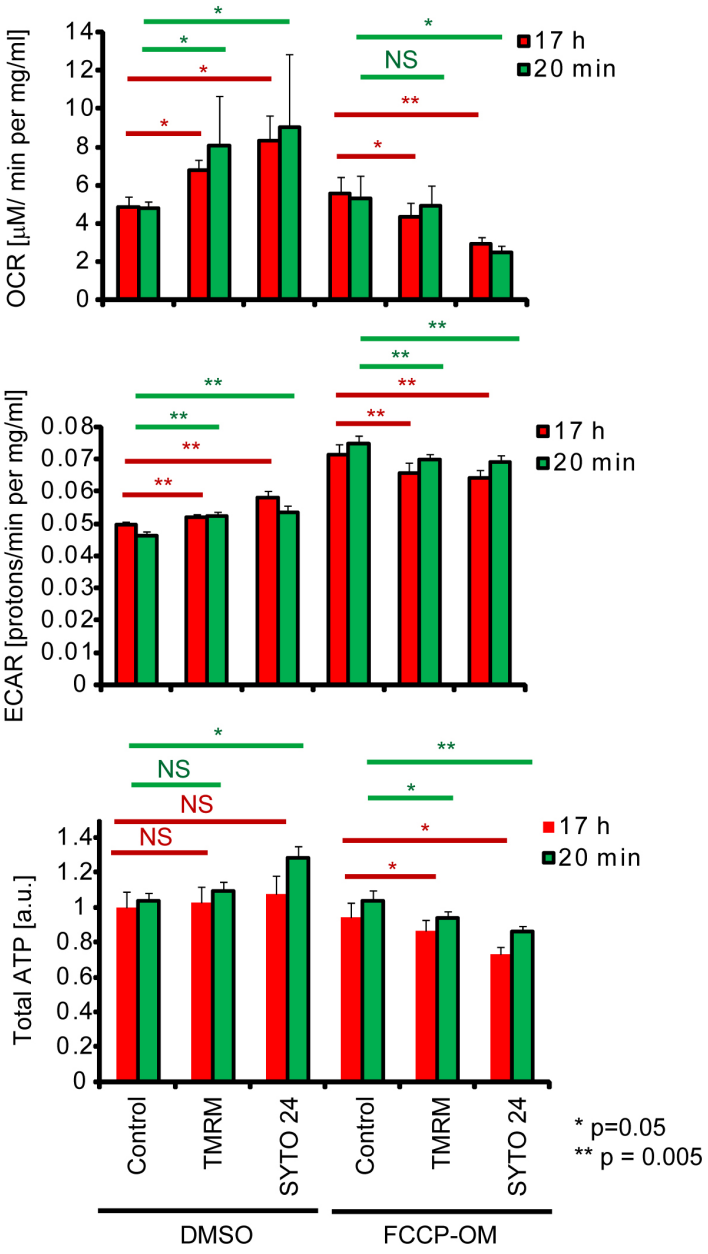

Figure 4. Evaluation of effects of SYTO 24 (0.1 µM) and TMRM (10 nM) staining on the bioenergetics of HCT116 cells. Cells were incubated with dyes for 20 min or 17 h and subjected to plate reader-based analysis of oxygen consumption rate (OCR), extracellular acidification rate (ECAR, glycolytic flux) and ATP at rest (DMSO treatment) or uncoupled conditions (1 µM FCCP – 10 µM oligomycin, FCCP-OM). A: OCR, N=6. B: ECAR, N=8. C: ATP, N=4. Presented data are normalized to total protein (BCA assay). NS-no statistically significant differences; asterisks indicate statistical differences (independent *t*-test).

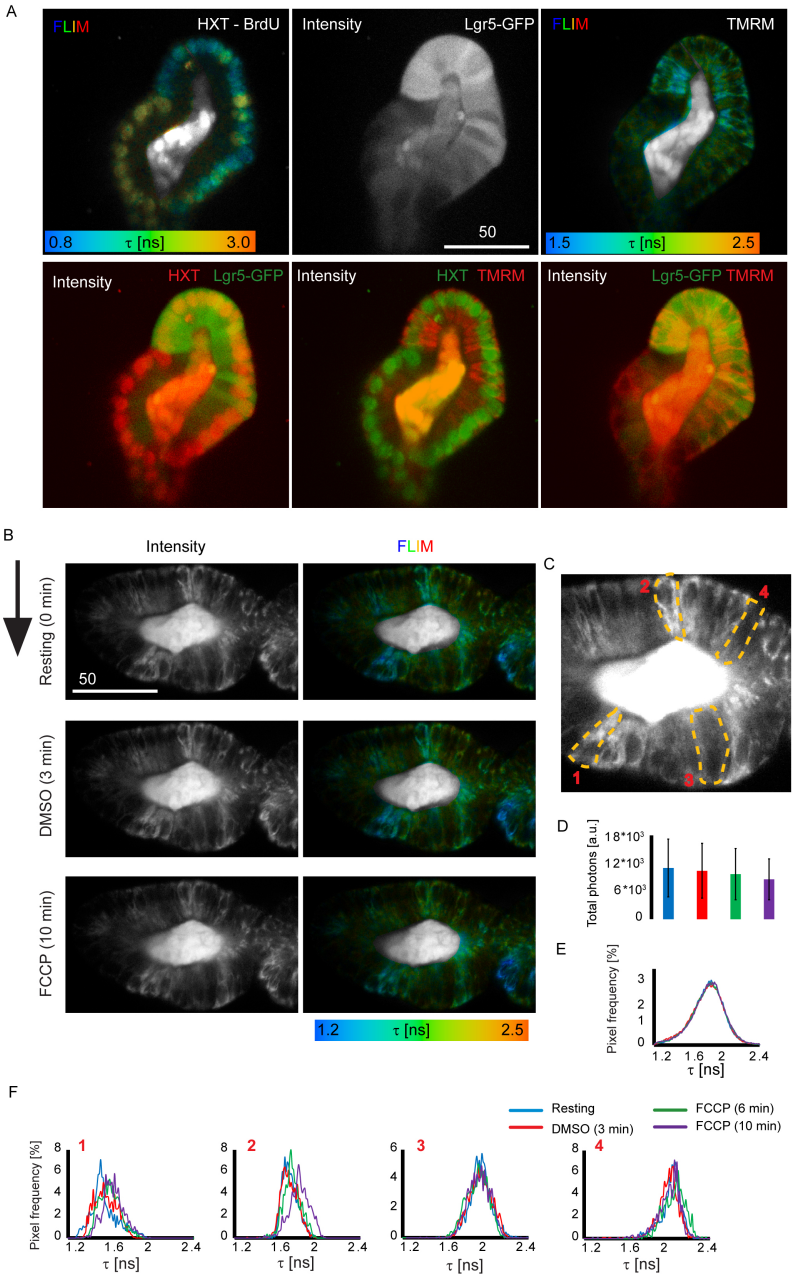

Figure 5. TMRM-FLIM of intestinal Lgr5-GFP organoids identifies differences in cell metabolism in stem cell niche. A: live images of Lgr5-GFP intestinal organoids, co-labeled with Hoechst 33342 – BrdU: decreased fluorescence lifetimes correspond to proliferating cells. Intensity and combined color-coded FLIM images are shown. Organoids were pulsed with 5 μM BrdU overnight (18 h) and stained with 2 μM Hoechst 33342 and 10 nM TMRM (1 h). TMRM was not present in the media during imaging. B-F: response to addition of 2 μM FCCP in organoids' chosen regions (C). D: photon intensity counts at the different stages of stimulation to DMSO (mock) and FCCP. E, F: Fluorescence lifetime distribution histograms

for the whole field (B) and selected (C) regions of interest during application of DMSO (mock) and FCCP. Scale bar is in µm.

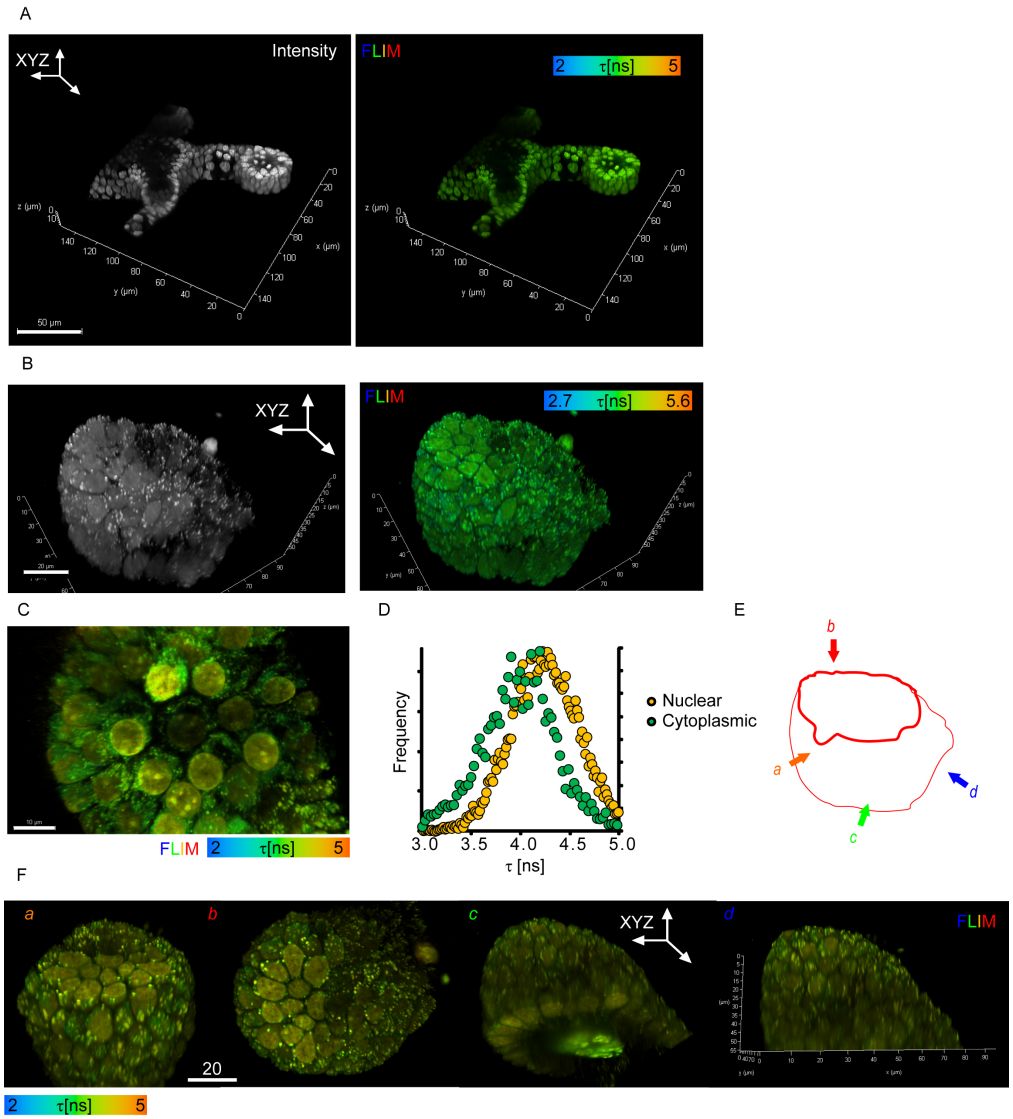

Figure 6. Staining and FLIM imaging of Lgr5-GFP organoids with SYTO 24 dye. A: Intensity (grayscale) and FLIM (color-coded scale) images of SYTO 24-stained and fixed organoids (3D reconstruction of 46 sections, Z=14.85 µm). B-F: live organoids stained with SYTO 24 (0.1 µM, 1 h). B: comparison of intensity (grayscale) and FLIM images (3D reconstruction of 79 sections, Z=54.6 µm). C: magnified view with modified color-coded scale revealing differences in the mitochondrial and nuclear decay times (3D reconstruction

of 37 sections, Z=18 μm). D: distribution histograms for a single cross-section from C, showing different fractions of fluorescence lifetimes. E, F: legend and different 3D views of live organoid imaged in FLIM (3D reconstruction of 79 sections, Z=54.6 μm).

Supplementary data

Estimation of the mitochondrial membrane potential using fluorescence lifetime imaging microscopy

Irina A. Okkelman[1], Dmitri B. Papkovsky[1*], Ruslan I. Dmitriev[1,2*]

[1]Laboratory of Biophysics and Bioanalysis, ABCRF, School of Biochemistry and Cell Biology, University College Cork, Cork, Ireland

[2]Institute for Regenerative Medicine, I.M. Sechenov First Moscow State University, Moscow, Russian Federation

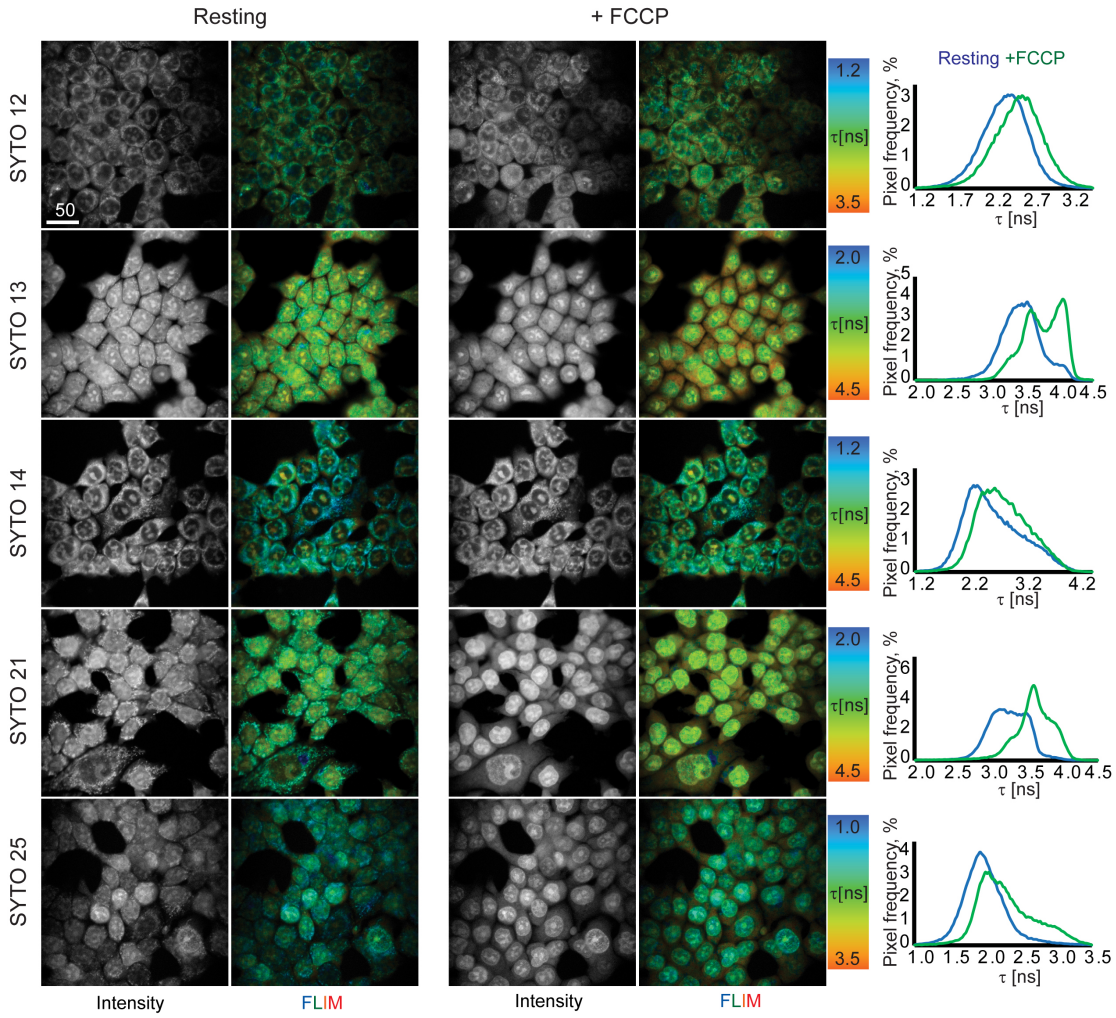

Figure S1. Fluorescence intensity and lifetime (FLIM) microscopy of live HCT116 cells stained with SYTO 12, 13, 14, 21 and 25 dyes (0.1 μM for 1 h, followed by washing). Grayscale fluorescence intensity and colored FLIM images and distribution histograms are shown. Scale bar is in μm.

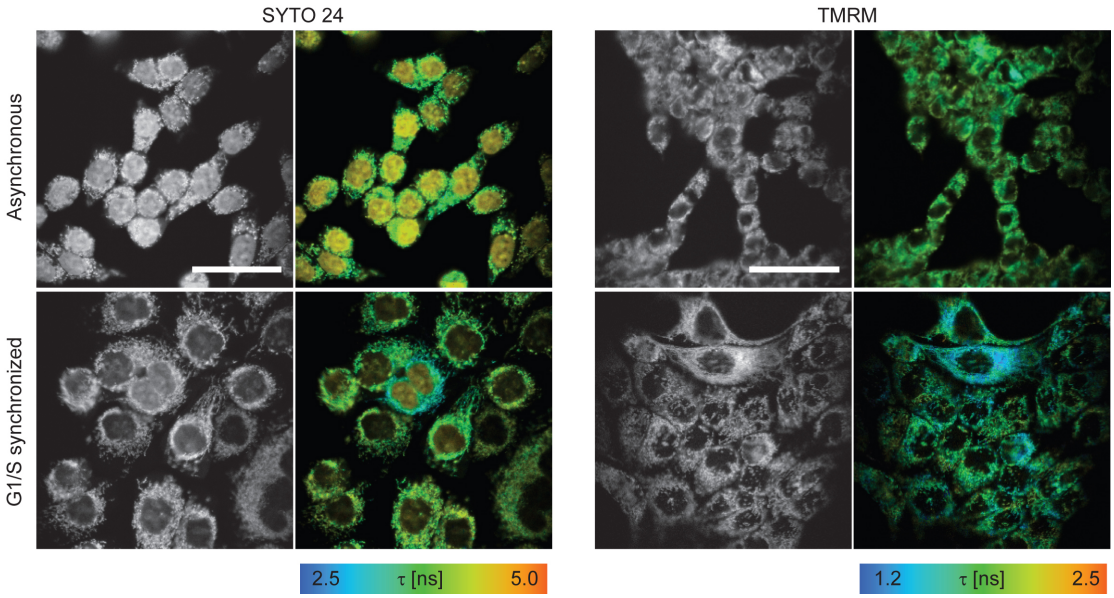

Figure S2. Mitochondrial morphology in asynchronous and G1/S-synchronized (1 µg/ml aphidicolin, 18 h) HCT116 cells stained with SYTO 24 (0.05 µM, 20 min) and TMRM (10 nM, left in imaging media). Scale bar is 50 µm.

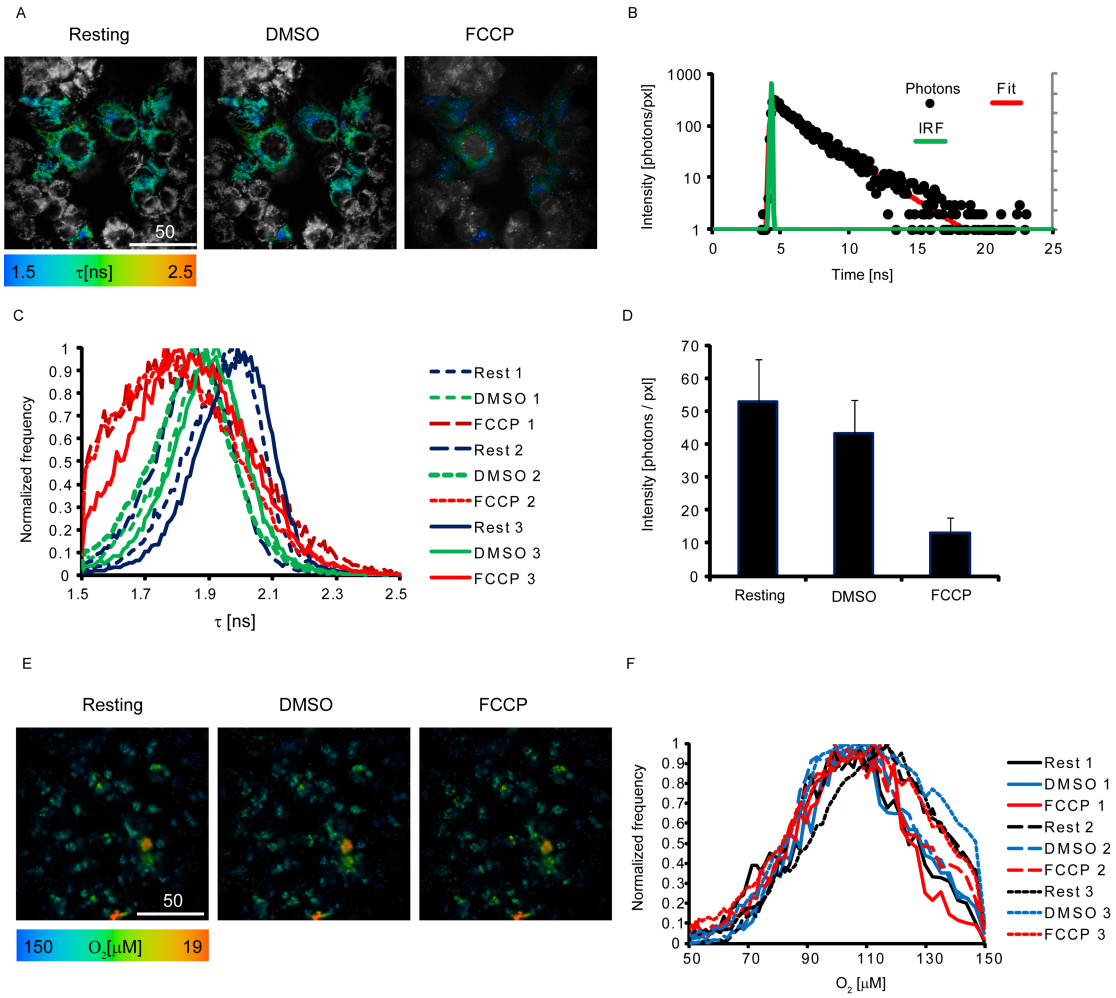

Figure S3. Response to membrane depolarization recorded by FLIM with TMRM dye in adherent culture of HCT116 cells. A: Combined intensity (grayscale) and FLIM data for cells stained with TMRM (10 nM, 15 min) at rest, upon addition of DMSO (mock) and 2 μM FCCP. B: example of fluorescence decay fitting for TMRM fluorescence (double-exponential fit). C: Distribution histograms for TMRM fluorescence decay time under different treatment conditions. N=3. D: Fluorescence intensity response to the treatment conditions for TMRM dye. E, F: Response to membrane depolarization recorded with the O_2-sensitive NanO2 probe by PLIM. Cells were stained with NanO2 (10 μg/ml, 16 h) and treated similarly to A-D. Phosphorescence lifetimes are converted to O_2 values. F: distribution histogram for observed oxygenation in response to FCCP treatment with NanO2-stained cells. N=3. Scale bar is in μm.

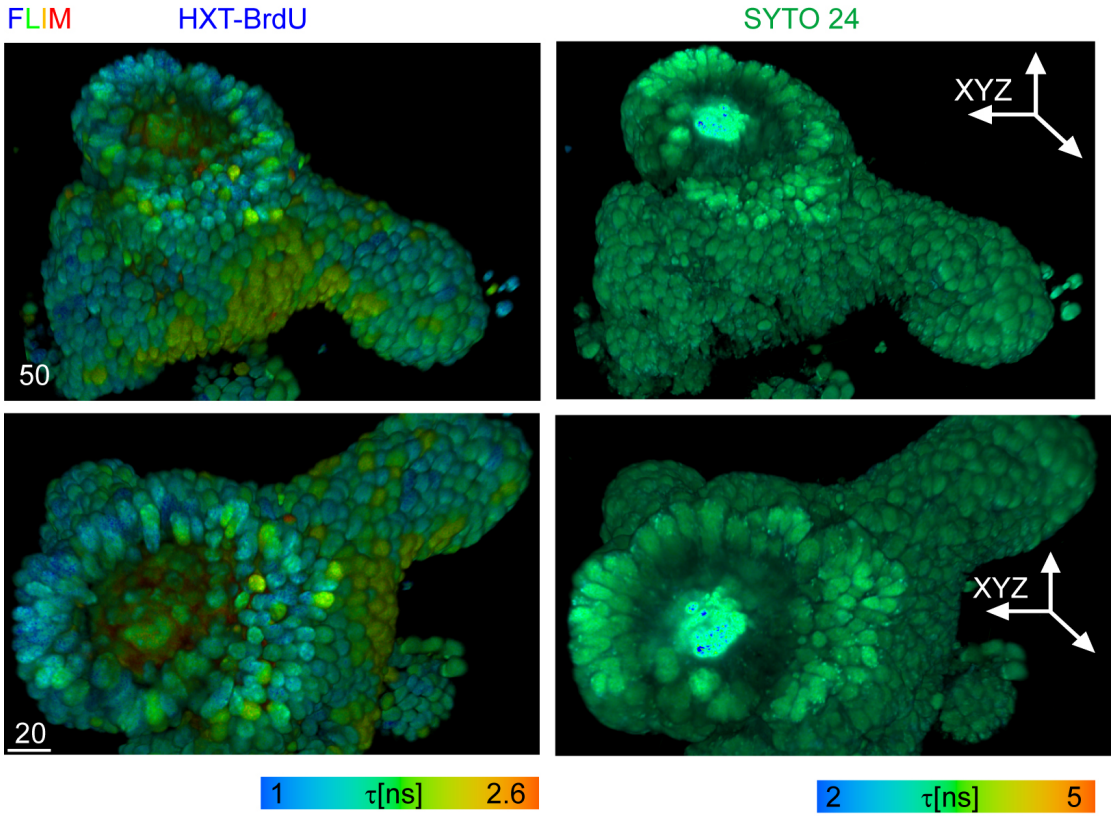

Figure S4. Sequential two-photon-excited FLIM imaging of intestinal organoids stained with Hoechst 33342 (2 μM, 2 h) / BrdU (5 μM, 18 h) and SYTO 24 (0.1 μM, 2 h) dyes. 3D reconstruction of FLIM images (96 sections, Z=94.9 μm) is shown. Scale bar is in μm.